Regional Cooperation for Limited Area modeling in Central Europe

GNSS slant total delays in the ALADIN NWP system: Phasing of the source code from cy40h1 to cy43t2

Report on stay at KNMI 28/10 – 22/11/2019

Martin Imrišek

Supervisor: Siebren de Haan
De Bilt 2019

Contents

Acknowledgement

I would like to thank my supervisor Siebren de Haan for his help and advices during my stay at KNMI. This stay was financed by Regional Cooperation for Limited Area modelling in Central Europe and by C-SRNWP Project in the form of the Short Term Scientific Mission. I would also like to thank my colleagues Maria Derková and Oldřich Španiel for their technical support.

1 Foreword

The Global Navigation Satellite System (GNSS) tropospheric products are becoming an important source of information of the water vapour distribution in the atmosphere. Nowadays various meteorological institutes utilize zenith total delay assimilation in their numerical weather prediction models. Next step is to utilize slant total delay data in assimilation as valuable source of information, which provides details about spatial distribution of water vapour. My stay at Koninklijk Nederlands Meteorologisch Instituut (KNMI) was focused on the implementation of the observation operator developed by Siebren de Haan from Aire Limitée Adaptation dynamique Développement InterNational (ALADIN) Numerical Weather Prediction (NWP) system cycle 40h1 to cycle 43t2. The main development was done in BATOR, SCREENING and MINIMISATION, more to be found in sections 3, 4 and 5. The BATOR stores the observations inside the domain of numerical weather prediction model to observational database. The SCREENING computes first guess departures to evaluate the discrepancy between numerical weather prediction model state and observations. After the SCREENING only suitable observations are stored for the MINIMISATION. Data are assimilated to numerical weather prediction model to improve the numerical weather prediction analysis in respect of initial state[1] and observations in the MINIMISATION step. At this stage of development all values of namelist variables are preliminary, not tested, nor recommended.

2 Introduction

The slant total delays are one of many derived products of the GNSS processing. The STD_k^i is integral delay caused by refraction of the GNSS signal in atmosphere transmitted from satellite i to receiver k on the Earth. Computation of slant total delay is based on the formula:

$$STD_k^i = mf_h(e)ZHD + mf_w(e)ZWD + mf_g(e)\left[G_N\cos(A) + G_E\sin(A)\right], \tag{1}$$

where

e is the elevation of GNSS signal,
A is the azimuth of GNSS signal,
mf_h is the coefficient of hydrostatic mapping function,
mf_w is the coefficient of wet mapping function,
mf_g is the coefficient of gradient mapping function estimated as:
$mf_g(e) = \frac{1}{sin(e)tan(e) + 0.0032}$ according to Chen & Herring (1997),
ZHD is the zenith hydrostatic delay,
ZWD is the zenith wet delay,
G_N is the north tropospheric gradient,
G_E is the east tropospheric gradient.

[1] Known also as background.

The ZHD, ZWD, G_N and G_E are estimated parameters from GNSS processing, while the mf_h, mf_w and mf_g are mapping functions estimated independently from GNSS observations, e.g. from in situ meteorological measurements (Saastamoinen, 1972) or from NWP models (Böhm *et al.*, 2006a) or (Böhm *et al.*, 2006b). The elevation e and azimuth A are derived from precise satellite and GNSS receiver coordinates. The tree terms of Eqn. 1 denote slant hydrostatic delay ($mf_h(e)ZHD$), slant wet delay ($mf_w(e)ZWD$) and gradient delay ($mf_g(e)\,[G_N \cos(A) + G_E \sin(A)]$). The schematic picture of slant total delays is displayed in Fig. 1.

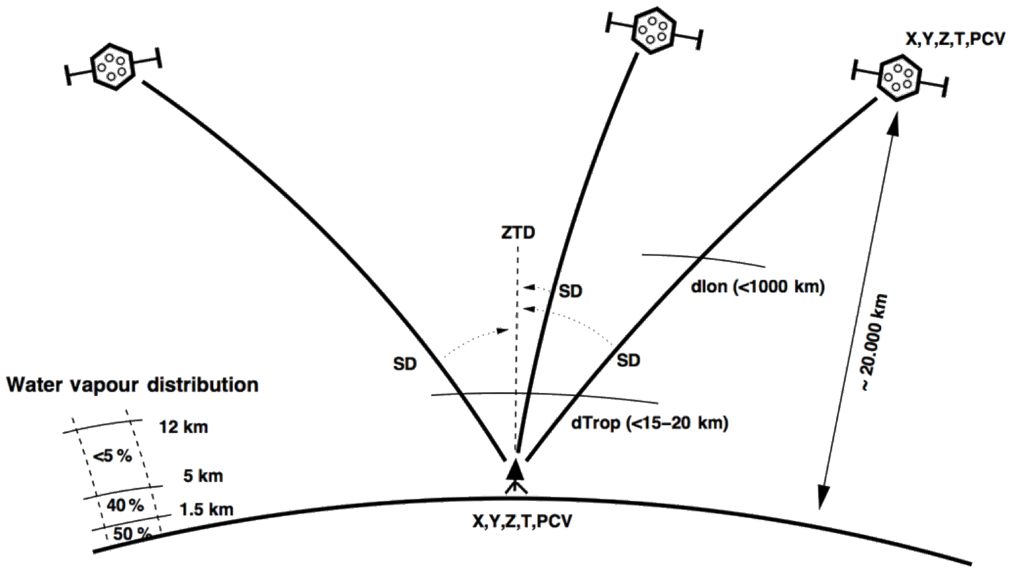

Figure 1: Schematic picture of slant total delays from Guerova *et al.* (2016).

The Zenith Hydrostatic Delay (ZHD) is caused by the dry gases present in the atmosphere. This component is relatively stable and can be sufficiently modelled. The hydrostatic delay is about 2.3 meters in zenith and about 10 meters in 10° elevation. On the other hand, the Zenith Wet Delay (ZWD) varies more with change of local weather conditions. This delay caused by water vapour and condensed water in form of clouds can vary from 0.1 meters in winter to 0.3 meters in summer.

The slant total delays for assimilation experiments were computed from GNSS near real time processing system of Department of Theoretical Geodesy a Slovak University of Technology in Bratislava. Various GNSS products are available at page space.vm.stuba.sk/pwvgraph/.

3 Bator

The code phasing from the cycle 40h1 to the cycle 43t2 bf10 was done in two separate packs on High Performance Computer (HPC) at Slovak Hydrometeorological Institute (SHMU). The list of changed/new source code files is in appendix A. The root pack contains development in Observational DataBase (ODB) and the local pack contains development in ARPIFS. This separation into two packs is recommended because the development of ODB should be independent from other development and this approach will speed up the compilation process of the code developed in ARPIFS. The latest version of source code is available at European Centre for Medium-Range Weather Forecasts (ECMWF) HPC */home/ms/sk/skj/pack-/source/cy43/SlantYYYYMMDD.tar*. More up to date information is to be found in the *README* file.

3.1 Input data

The OBSOUL conventional data format is used to store the Slant Total Delay (STD) data, as is shown[2] in the Lis. 1.

```
    20190824 00
    17 19 111 48.751804 19.151007 'BBYSSUT_' 20190824 000000 448.183 1 11111 0
    129 165.186112 64.179396 2.681502 1.003

         NSTD                          NCINLV - number of slants/ROBODY-s  NCISTD
    NGNSS   |       LAT       LON station id     date  time altitude |  Flag |
        |   |         |         |          |        |     |        | |     | |
    17 19 111 48.751804 19.151007 'BBYSSUT_' 20190824 000000 448.183 1 11111 0 -- header
                           satellite number
    ASTD   azimuth elevation      STD | error
      |          |         |        | |   |
    129 165.186112 64.179396 2.681502 1.003                                    -- body
```

Listing 1: The example of OBSOUL.conv file

In this version of the code, only **one** body is allowed per header. The latitude, longitude, azimuth and elevation angle are stored in degrees and the altitude STD and formal error are stored in metres. The values of STD and its formal observation error are mapped to given azimuth and elevation angle. The satellite number is combined with the observation error in the last column of body. The integer part is reserved for the satellite number and the decimal part for the STD error. The formal error from GNSS post processing should not exceed few centimetres even at low elevation angle.

The OBSOUL data are read in *bator_lectures_mod.F90*[3] as conventional data *OBSOUL.conv*. It is mandatory to define the input data format for BATOR via the *batormap* file as is shown in the Lis. 2.

```
conv     conv     OBSOUL   conv
```

Listing 2: The *batormap* file example

The OBSOUL data are separated[4] and stored to ODB in *bator_ecritures_mod.F90*.

[2] First tree lines.
[3] Without any modification.
[4] Satellite number and STD error.

3.2 Observational DataBase

New fields related to STD were added to BODY table:

- MDB_SATID_AT_BODY – Satellite identifier, meant to be used for satellite blacklisting[5],
- MDB_AZIMUTH_AT_BODY – Azimuth of satellite at GNSS permanent station,
- MDB_ELEVATION_AT_BODY – Elevation angle of satellite at GNSS permanent station,
- MDB_REFCONST_AT_BODY – Refractivity constant C at GNSS permanent station. It is set to -999.9 in BATOR, computed in *gnss_slant_delay.F90* as: $C = n_0 sin(\alpha_0)$,
  n_0 is refractivity at GNSS permanent station,
  α_0 is model (real) elevation angle of GNSS signal at permanent station.
- MDB_PHI_AT_BODY – geocentric angle between GNSS permanent station and GNSS satellite. It is set to -999.9 in BATOR, computed in *gnss_slant_delay.F90*.

The data can be retrieved from ODB database in two ways. The name of database variable depends on variable in *ctxinitdb.F90*. The example of old ODB request is in Lis. 3, while the new ODB request is in Lis. 4.

```
ZREFCON = ROBDDR(MLNKH2B(IOBSPO),MDB_REFCONST_AT_BODY)
```

Listing 3: Example of old ODB request

```
USE ODB_INTERFACE, ONLY: AVIEW
.
.
.
ZREFCON = ROBODY%DATA(IOBS,ROBODY%REFCONST_AT_BODY)
```

Listing 4: Example of new ODB request

3.3 Other notes

- The actual name of database in Fortran routines is derived from *view name* and *view ncase* in *ctxinitdb.F90*.
- Setup of the MDBOER[6] is done in *bator_ecritures_mod.F90* without applying the SIGMAO_COEF. Application of the SIGMAO_COEF and computation of MDBFOE[7] is done in *hop.F90/obsop_gnss.F90/gnss_oberror.F90*. The change of default SIGMAO_COEF variable from value 1.0 to 2.0 can by done in namelist *fort.4*, as is shown in the Lis. 5.

```
&NAMCOSJO
  SIGMAO_COEF(19)=2.00,
/
```

Listing 5: New SIGMAO_COEF variable in *fort.4* file for SCREENING

This namelist variable is optional.

[5]Not yet implemented.
[6]Observation error.
[7]Final error.

- The new observation type GNSS (19) and new observation STD (129) were added. One can follow this development by searching for variables NGNSS and NSTD in the source code.
- Its highly recommended to clean pack after any development in ODB and then compile.
- Each new Structured Query Language (SQL) request has to be included in *ctxinitdb.F90*.

4 Screening

The discretization in model space along the signal path by routines *mkglobstab_obs.F90* and *mkglobstab_model.F90* is necessary before the computation of the first guess value by observation operator H. After the development of model space discretization the *hop.F90* routine was modified to call *obsop_gnss.F90* in case of STD observation where observation error, final error and first guess value are computed.

4.1 Discretization of model space

The main development was done in *mkglobstab_obs.F90* and *gnss_plane.F90* routines. The number of vertical profiles in model space is set by namelist variable, as is shown in the Lis. 6.

```
1 &NAMNPROF
2   NOBSPROFS(19)=87,
3 /
```

Listing 6: New NOBSPROFS variable in *fort.4* file for SCREENING

In this case the number of profiles is set to number of vertical levels. The default value for any NOBSPROFS variable is 1, however this value is not permitted for slant total delay observation operator. It is mandatory to introduce this variable to SCREENING and MINIMISATION namelists, the value can differ in these configurations. The impact of number of profiles on assimilation will be object of further testing.

4.2 Observation operator

The computation of the slant total delay first guess value is done in the observation operator routine *hop.F90/obsop_gnss.F90/gnss_slant_delay.F90* according to the data flow in cycle 43[8]. The model (real) elevation angle from GNSS station to satellite is computed from the model state and the Snell's law. Model elevation angle is compared to geometric (true) elevation angle until the difference or number of iterations is satisfied. The iterations of model signal path are displayed in Fig. 2 where:

- φ is the geocentric angle from GNSS station to satellite,
- $\Delta\varphi_k$ is the difference of geocentric angles between two intersections of GNSS signal and model levels,
- h_{top} is the level closest to satellite where the signal is bent for the last time. It is not part of the model, the altitude is set to 75 km.

[8] After the OOPS–ification of the code.

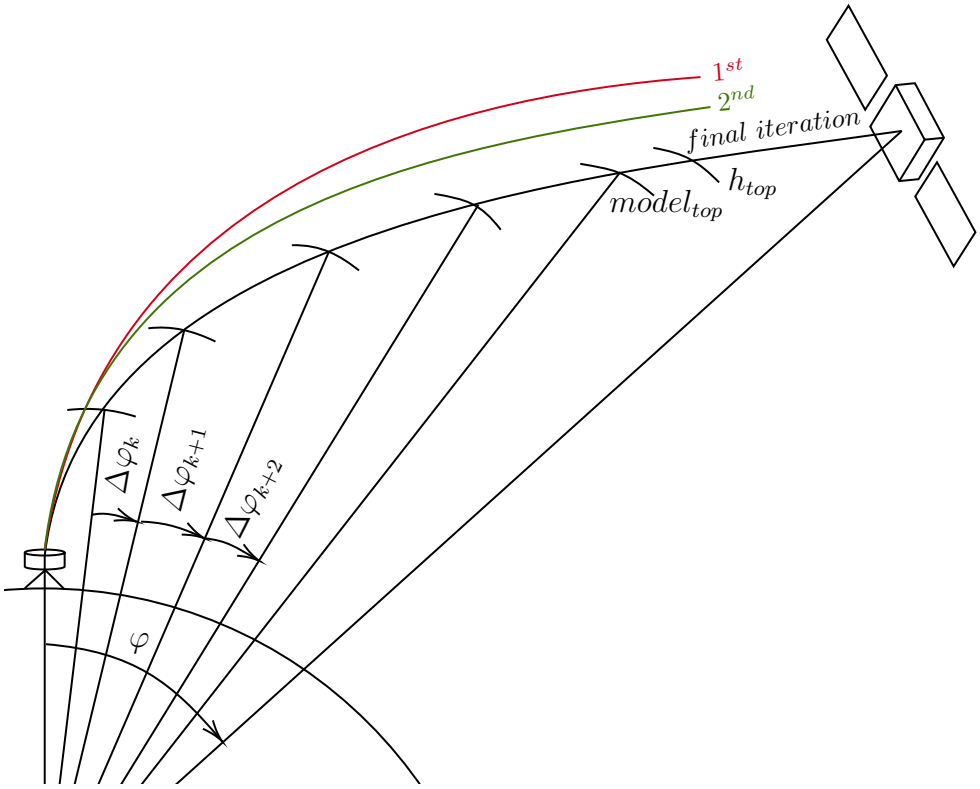

Figure 2: GNSS signal path.

The GNSS signal ray tracing flow chart is in appendix B. After the real elevation angle is obtained the slant total can be estimated with formula Eqn. 2.

$$STD = \sum_k \sqrt{G_k^2}\,(D_k + 1) \tag{2}$$

where

k is the index of model level,
the geometric part of equation:

$$G_k^2 = H_k^2 - 2H_kH_{k+1}cos(\varphi_k) + H_{k+1}^2 + 2R_e^2(1-cos(\varphi_k)) + 2R_e(H_k+H_{k+1})(1-cos(\varphi_k)) \tag{3}$$

H_k is the altitude of intersection of model level and signal path,
R_e is the Earth radius, defined in *sucst.F90*,
φ_k is the geocentric angle of intersection of model level and signal path and GNSS station.

the physical part of equation:

$$D_k = \frac{(p_k - e_k)\,k_1}{T_k} + \frac{e_k k_2}{T_k} + \frac{e_k k_3}{T_k^2} \tag{4}$$

k_1 is the physical constant of refraction, defined in *sucst.F90*,

k_2 is the physical constant of refraction, defined in *sucst.F90*,
k_3 is the physical constant of refraction, defined in *sucst.F90*,
T_k is the temperature at intersection of model and signal path,
p_k is the atmospheric pressure at intersection of model and signal path,
e_k is the water vapour pressure at intersection of model and signal path.

4.3 Other notes

- New constants related to STD estimation were introduced to compute STD model value in observation operator. The declaration is in *yomcst.F90*, while the values are introduced in *sucst.F90*.
- The setup of STD error limits is in *defrun.F90*, as is shown in the Lis. 7. Based on these limits (RBGQC) the first guess departures are tested and possibly rejected in SCREENING due to *8= TOO BIG FIRST GUESS DEPARTURE*.

```
!* Slant GNSS
LVARQC(NVAR_SPD,NGNSS )=.TRUE.
RAQC  (NVAR_SPD,NGNSS )=0.01_JPRB
RLQC  (NVAR_SPD,NGNSS )=5.0_JPRB
RBGQC (NVAR_SPD,NGNSS ,1:3) = (/9.00_JPRB,16.0_JPRB,25.0_JPRB/)*100.5_JPRB
```

Listing 7: The part of *defrun.F90* file

  Coefficients RAQC and RLQC are the same as for Zenith Total Delay (ZTD). The values of the coefficients and the factor of the RBGQC array will be subject of further testing and investigation.
- Several modification were made to print out information about usage of observation in screening output.

5 Minimisation

The introduction to this section is based on ECMWF (2017) data assimilation documentation. In Three–Dimensional Variational analysis (3D–Var) an objective function J is minimized. The cost function consists of these terms:

$$J = J_b + J_o + J_q + J_c \tag{5}$$

measuring, respectively, the discrepancy with the background (a short-range forecast started from the previous analysis), J_b, with the observations, J_o, with the model error, J_q, and with the slow manifold of the atmosphere, J_c. The J_c term controls the amplitude of fast waves in the analysis. The last two terms are omitted from the subsequent derivations in this section.

In its incremental formulation (Courtier *et al.*, 1994), we write

$$J(\delta\mathbf{x}) = \frac{1}{2}\delta\mathbf{x}^T\mathbf{B}^{-1}\delta\mathbf{x} + \frac{1}{2}(\mathbf{H}\delta\mathbf{x} - \mathbf{d})^T\mathbf{R}^{-1}(\mathbf{H}\delta\mathbf{x} - \mathbf{d}) \tag{6}$$

where $\delta\mathbf{x}$ is the increment. At the minimum of $J(\delta\mathbf{x})$ the resulting analysis increment $\delta\mathbf{x}^a$ is added to the background $\mathbf{x}^b$ in order to provide the analysis $\mathbf{x}^a$ given by

$$\mathbf{x}^a = \mathbf{x}^b + \delta\mathbf{x}^a \tag{7}$$

$\mathbf{B}$ is the covariance matrix of background error while $\mathbf{d}$ is the innovation vector

$$\mathbf{d} = \mathbf{y}^o + H\mathbf{x}^b \tag{8}$$

where $\mathbf{y}^o$ is the observation vector. $\mathbf{H}$ is a suitable low-resolution linear approximation of the observation operator H in the vicinity of $\mathbf{x}^b$, and $\mathbf{R}$ is the covariance matrix of observation errors. The incremental formulation of 3D–Var consists therefore of solving for $\delta\mathbf{x}$ the inverse problem defined by the (direct) observation operator $\mathbf{H}$, given the innovation vector $\mathbf{d}$ and the background constraint.

The tangent linear observation operator $\mathbf{H}$ is developed in the *gnss_slant_delaytl.F90* routine. The slant total delay τ depends on model state $\mathbf{x}$ at k and $k-1$ levels and refractivity constant C. Multiple functions[9] $\mathbf{f}$ are used to estimate slant total delay

$$\tau = \sum_k f^k(\mathbf{x}_k, \mathbf{x}_{k-1}, C). \tag{9}$$

The considered levels k are: interpolated model state at GNSS station, model levels above the station, atmospheric state at h_{top}. The tangent linear τ is obtained by differentiating Eqn. 9 with respect to $\mathbf{x}$ and C

$$\delta\tau = \sum_k \left(\mathbf{G}_k^k \delta\mathbf{x}_k + \mathbf{G}_{k-1}^k \delta\mathbf{x}_{k-1} + \frac{\partial f^k}{\partial C}\delta C \right), \tag{10}$$

where $\mathbf{G}_j^i = \dfrac{\partial f^i}{\partial \mathbf{x}_j}$. The geocentric angle φ is constant for STD

$$\varphi = \sum_k \varphi^k \left(\mathbf{x}_k, \mathbf{x}_{k-1}, C\right), \tag{11}$$

its partial derivative is equal to

$$\delta\varphi = \sum_k \left(\frac{\partial\varphi^k}{\partial\mathbf{x}_k}\delta\mathbf{x}_k + \frac{\partial\varphi^k}{\partial\mathbf{x}_{k-1}}\delta\mathbf{x}_{k-1} + \frac{\partial\varphi^k}{\partial C}\delta C \right) = 0. \tag{12}$$

The tangent linear C obtained from Eqn. 12 is

$$\delta C = -\left(\sum_k \frac{\partial\varphi^k}{\partial C} \right)^{-1} \sum_k \left(\frac{\partial\varphi^k}{\partial\mathbf{x}_k}\delta\mathbf{x}_k + \frac{\partial\varphi^k}{\partial\mathbf{x}_{k-1}}\delta\mathbf{x}_{k-1} \right). \tag{13}$$

The computation of linear approximation of slant total delay is done in two steps. In the first step the term related to refractivity C is computed (Eqn. 14). The index i denotes model level as k, but is computed in separate summation

[9] Different function for $model_{top} \to h_{top}$ layer is used.

$$REF = \sum_k \frac{\partial f^k}{\partial C} \left(- \sum_i \frac{\partial \varphi^i}{\partial C} \right)^{-1} . \tag{14}$$

In the second step the tangent linear of slant total delay $\delta\tau$ is computed. The formula based on Eqn. 10, 13 and 14 is

$$\delta\tau = \sum_k \left(\mathbf{G}_k^k \delta\mathbf{x}_k + \mathbf{G}_{k-1}^k \delta\mathbf{x}_{k-1} \right) + REF \sum_k \left(\frac{\partial \varphi^k}{\partial \mathbf{x}_k} \delta\mathbf{x}_k + \frac{\partial \varphi^k}{\partial \mathbf{x}_{k-1}} \delta\mathbf{x}_{k-1} \right) . \tag{15}$$

$$\delta\tau = \sum_k \left[\left(\mathbf{G}_k^k + REF \frac{\partial \varphi^k}{\partial \mathbf{x}_k} \right) \delta\mathbf{x}_k + \left(\mathbf{G}_{k-1}^k + REF \frac{\partial \varphi^k}{\partial \mathbf{x}_{k-1}} \right) \delta\mathbf{x}_{k-1} \right] . \tag{16}$$

With $\boldsymbol{B}^k = \mathbf{G}_k^k + REF \frac{\partial \varphi^k}{\partial \mathbf{x}_k}$ and $\boldsymbol{C}^k = \mathbf{G}_{k-1}^k + REF \frac{\partial \varphi^k}{\partial \mathbf{x}_{k-1}}$ we can 16 simplify as

$$\delta\tau = \sum_k \left(\boldsymbol{B}^k \delta\mathbf{x}_k + \boldsymbol{C}^k \delta\mathbf{x}_{k-1} \right) . \tag{17}$$

If we reorder the summation in respect for the increments of the same model level and if we consider the bottom coefficient $\boldsymbol{C}^{k_{max}+1} = 0$ we get

$$\boxed{\delta\tau = \sum_k \left(\boldsymbol{B}^k \delta\mathbf{x}_k + \boldsymbol{C}^{k+1} \delta\mathbf{x}_k \right) .} \tag{18}$$

The adjoint version of observation operator is developed in the routine *gnss_slant_delayad.F90*. The incremental model state for level k is equals

$$\boxed{\delta x_k = \boldsymbol{B}^k \delta\tau + \boldsymbol{C}^{k+1} \delta\tau .} \tag{19}$$

It is mandatory to switch on[10] the use of STD observations type variable in J_o. This is done with NOTVAR variable in minimisation namelist.

```
&NAMCOSJO
  NOTVAR(1,19)=-1,-1,-1,-1,-1,-1,-1,-1,-1,-1,-1,-1,-1,-1,-1,-1,-1,0,-1,-1,-1,-1,-1,-1,
/
```

Listing 8: New NOTVAR variable in *fort.4* file for MINIMISATION

In this case only the specific humidity is considered in J_o for slant total delay. More details in *yomcosjo.F90*.

5.1 Other notes

- In the current version of the code the *no optimize* adjustment

```
!DEC$ NOOPTIMIZE
```

Listing 9: No optimize adjustment

[10] The value is set to 0.

has to be added in *obsop_gnss.F90* and *gnss_slant_delayad.F90* routines on top of the routine, right below the input/output parameters. Without this modification the minimisation of multiple slants is not possible.

6 Experiments

These results of experiments are preliminary and they can change with further development of the code.

6.1 Model description

The assimilation experiments were done on old the operational ALADIN/CHMI NWP setup[11]:

- ALadin–AROme (ALARO)-1 physic,
- domain: Δx 4.7 km, 529x421 grid points,
- 87 vertical levels, model top 49 555 m.

6.2 Assimilation of single slant total delay

As the first experiment the assimilation of only one randomly chosen STD from GNSS station BASV (Banská Štiavnica) at 00 UTC on 7 January 2019 was performed. The analysis departure is one order of magnitude smaller compared to the first guess departure. The increments of specific humidity are displayed in Fig. 3, 4 and 5.

```
statid@hdr lat@hdr lon@hdr stalt@hdr date@hdr time@hdr azimuth@body elevation@body
    obsvalue@body  final_obs_error@errstat an_depar@body fg_depar@body
'BASVSUT_' 48.447763 18.921021 578.130571 20190107 000000 174.904261 16.842768 7.481733 0.0162
     0.00048032649945817 0.0043810290293695
```

Listing 10: ODB output from CCMA after MINIMISATION

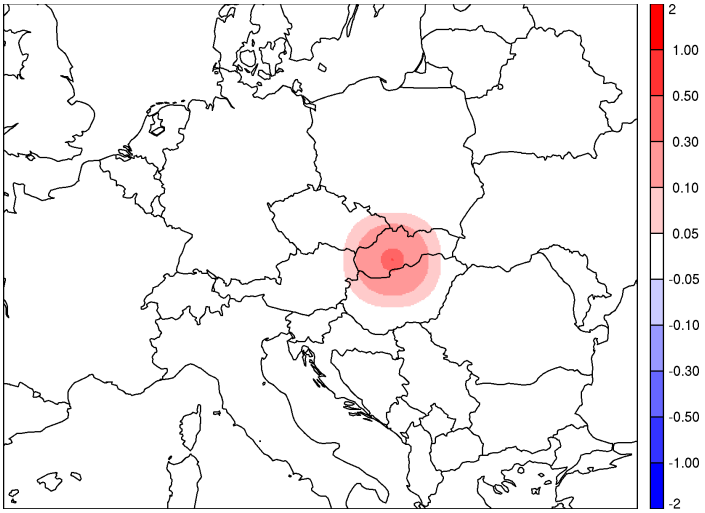

Figure 3: Increments of specific humidity [0.1 g kg^{-1}] at model level 60 of single STD assimilation at station BASV at 00 UTC on 7 January 2019.

[11] More info: www.umr-cnrm.fr/aladin/IMG/pdf/czstatus.pdf

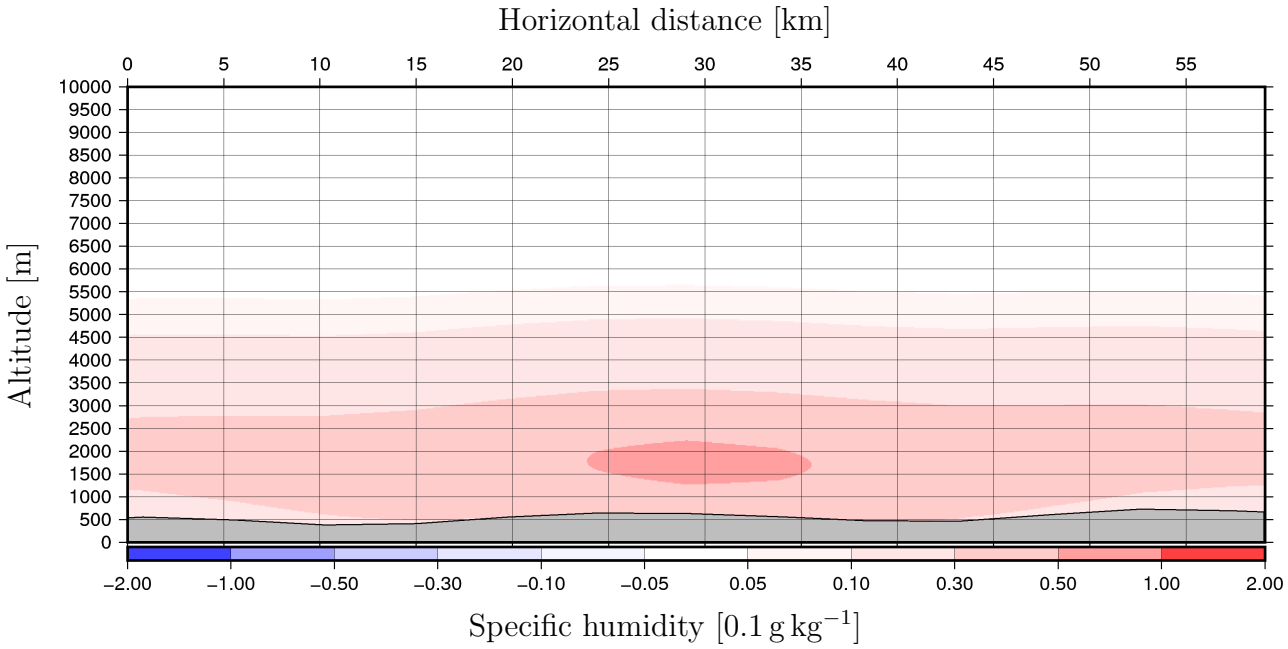

Figure 4: Vertical east–west cross section of increments of specific humidity [0.1 g kg^{-1}] at 00 UTC on 7 January 2019.

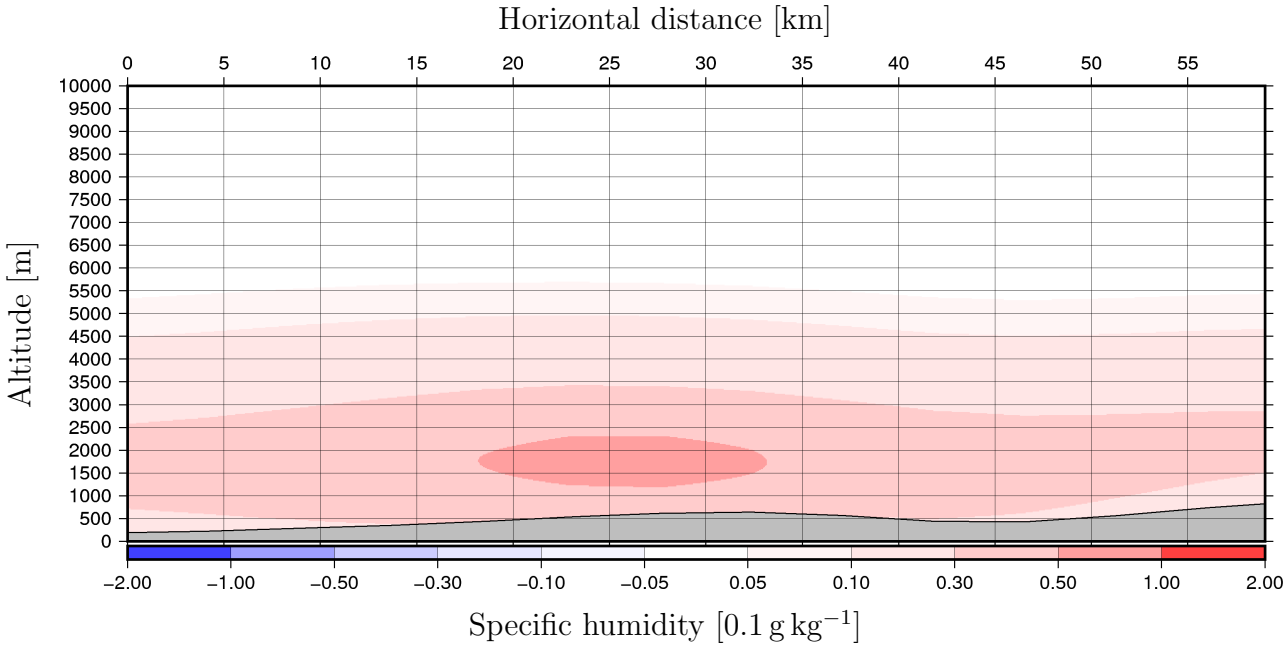

Figure 5: Vertical north–south cross section of increments of specific humidity [0.1 g kg^{-1}] at 00 UTC on 7 January 2019.

The horizontal (Fig. 3) and vertical (Fig. 4 and Fig. 5) increments look similar like increments from single ZTD assimilation, but in this case they are stretched in north–west direction.

6.3 Assimilation of all slant total delays from one station

The assimilation of all available STDs from GNSS station BASV was performed, the increments of specific humidity are displayed in Fig. 6. The positive increments[12] are located mainly on east of the station. Actually, some negative increments were noticed on west of the station. Asymmetrical increments at GNSS station are expected feature of assimilation of all available slant total delays at GNSS station.

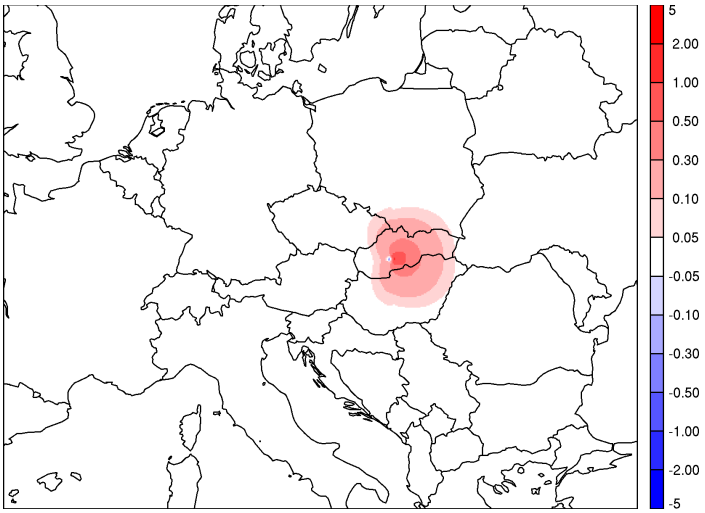

Figure 6: Increments of specific humidity [0.1 g kg^{-1}] at model level 60 of all STDs assimilation at station BASV at 00 UTC on 7 January 2019.

6.4 Assimilation of all slant total delays from all station

The assimilation of all available STDs from 7 January 2019 00 UTC was done. Overall 714 STDs from 22 GNSS permanent stations were assimilated. The increments of specific humidity are displayed in Fig. 7.

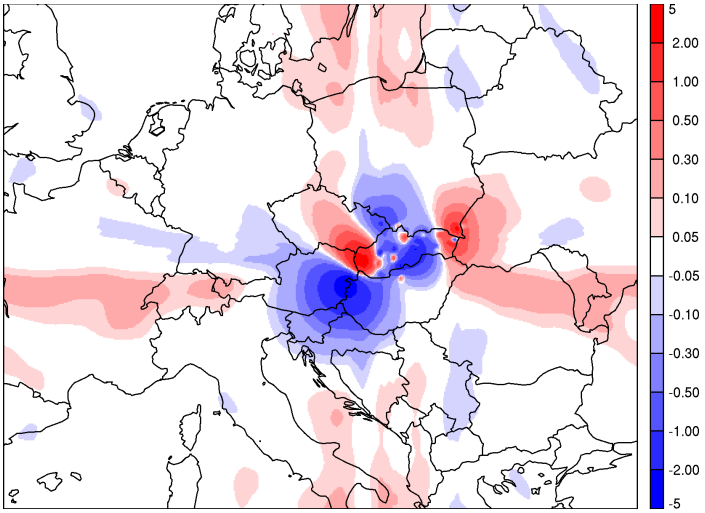

Figure 7: Increments of specific humidity [0.1 g kg^{-1}]at model level 60 of STDs assimilation at all stations at 00 UTC on 7 January 2019.

[12]More specific humidity in analysis.

6.5 Assimilation of all available observations

The full observation experiment[13] (FULL) and the same experiment without STDs (FULL–STD) were done to examine the minimisation behaviour of full assimilation experiment. The differences in increments of specific humidity of FULL and FULL–STD experiments are displayed in Fig. 8.

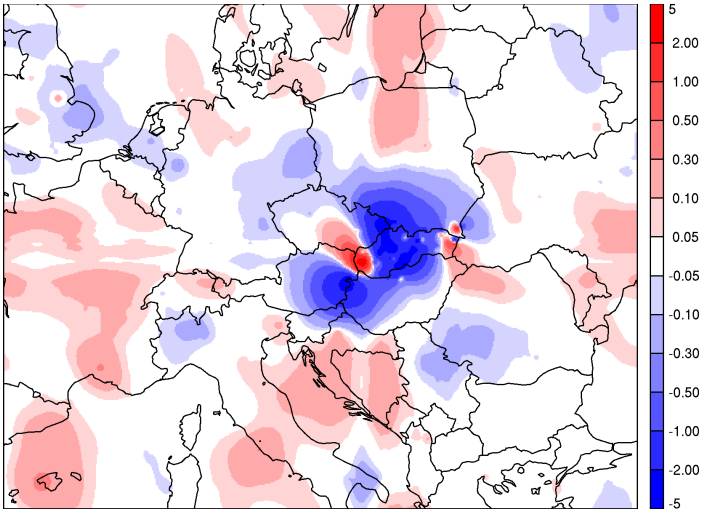

Figure 8: Increments differences of specific humidity $[0.1\,\mathrm{g\,kg^{-1}}]$ at model level 60 between FULL and FULL–STD assimilation at 00 UTC on 7 January 2019.

The increments of specific humidity are present in locations where no STDs were assimilated. This phenomena will be subject of further investigation. It may be caused by memory management, optimization or vectorization of the code.

Also, the FULL–STD experiment was compared to reference experiment with executable from export version cycle 43t2 bf10. The results are not equal. However, the J_o cost function for all observation types after minimisation have nine equal significant figures, and the SP NORMS 3D have also nine equal significant figures. This discrepancy will be subject of further investigation.

[13] SYNOP, TEMP, AMW, AMDAR, STD.

7 Conclusion

The Siebren de Haan's development in utilization of STD in NWP system ALADIN was introduced to the cycle 43t2 bf10 after one month stay at KNMI and consequential work. The development was technically tested with minor success. The increments in specific humidity from assimilation of one STD at station, all STDs at station and all STDs at all stations are looking promising. Nevertheless, further development and testing are necessary.

8 Outlook

The work on this topic will be ongoing in the future. These improvements, tests of code and validations are proposed:

- To solve the code optimization issue.
- To perform the tangent linear and adjoint tests.
- Setup the rejection criterion of the first guess departures (RBGQC).
- The new ODB fields related to STD should be moved from BODY to separate table dedicated to GNSS observations.
- More BODYs from the same GNSS station should be stored under one HEADER in ODB.
- To add differential slant total delay as new observation to observation type GNSS (19).
- To add slant total delays to BUFR format.
- Merge ZTD and STD into one observation type GNSS (19).
- Investigate the possibility of blacklisting of STDs based on elevation angle.
- To study the long term impact of assimilation of STDs on NWP forecast.
- Implementation of development to the latest possible export cycle, once the STD development will be validated.

Bibliography

Böhm, J., Niell, A. E., Tregoning, P., & Schuh, H. 2006a. Global Mapping Function: A new empirical mapping function based on numerical weather model data. *Geophysical Research Letterss*, **33**.

Böhm, J., Werl, B., & Schuh, H. 2006b. Troposphere mapping functions for GPS and VLBI from ECMWF operationals analysis data. *Journal of Geophysical Research*, **111**.

Chen, G., & Herring, T. A. 1997. Effects of atmospheric azimuthal asymmetry on the analysis of space geodetic data. *Journal of Geophysical Research*, **1022(B9)**, 20489–20502.

Courtier, P., Thépaut, J.-N., & Hollingsworth, A. 1994. A strategy for operational implementationof 4D–Var, using an incremental approach. *Quarterly Journal of the Royal Meteorological Society*, **120**, 1367–1388.

ECMWF. 2017. PART II: DATA ASSIMILATION. *IFS DOCUMENTATION – Cy43r3*, 103.

Guerova, G., Jones, J., Dousa, J., Dick, G., de Haan, S., Pottiaux, E., Bock, O., Pacione, R., Elgered, G., Vedel, H., & Bender, M. 2016. Review of the state-of-the-art and future prospects of the ground-based GNSS meteorology in Europe. *Atmospheric Measurement Techniques*, **9**, 5385–5406.

Saastamoinen, J. 1972. Atmospheric Correction for the Troposphere and Stratosphere in Radio Ranging Satellites. *The Use of Artifical Satellites for Geodesy in Geodesy*, **15**, 247–251. Washington, D.C.

Appendices

A List of changed/new source code files

odb/cma2odbgetdb.F90
odb/cma2odb/initmdb.F90
odb/cma2odb/ctxinitdb.F90
odb/ddl/body.h
odb/ddl/radiance_averaging.sql
odb/ddl/robody.sql
odb/ddl/robody_min.sql
odb/ddl/obsmon_sat.sql
odb/ddl/count_orbit.sql
odb/ddl/ralt_wam.sql
odb/ddl/getgnssid.sql
odb/ddl/obstype.h
odb/ddl/suobarea_gnss.sql
odb/ddl/suobarea.sql
odb/ddl/body_gnss.sql
odb/ddl/obsort_gnss.sql
odb/ddl/mkglobstab_gnss.sql
odb/ddl/black_robhdr_10.sql
odb/ddl/black_robody_10.sql
odb/ddl/black_robhdr_11.sql
odb/ddl/black_robody_11.sql
odb/include/compat_fill_mdb_members.h
odb/include/compat_mdb_members.h
odb/include/odb_assoc_cols.h
odb/include/odb_it_members.h
odb/module/varindex_module.F90
odb/pandor/module/bator_util_mod.F90
odb/pandor/module/bator_saisies_mod.F90
odb/pandor/module/bator_impr_mod.F90
odb/pandor/module/bator_ecritures_mod.F90
odb/pandor/module/bator_pool_balance_mod.F90

arpifs/common/yomdb_defs.h
arpifs/common/yomdb_vars.h
arpifs/common/yomdb_defs_undef.h
arpifs/canari/caratk.F90
arpifs/canari/capito.F90
arpifs/module/yomcoctp.F90
arpifs/module/varno_module.F90
arpifs/module/pardimo.F90
arpifs/module/yomcosjo.F90
arpifs/module/yomgnss.F90
arpifs/module/yomcst.F90
arpifs/module/yomcmddr.F90
arpifs/setup/cmoctmap_inv.F90
arpifs/setup/cmoctmap.F90
arpifs/setup/su_events.F90
arpifs/setup/sucmahop.F90
arpifs/setup/sucmad1.F90
arpifs/setup/suvnmb.F90
arpifs/setup/sucst.F90
arpifs/var/sualcosjo.F90
arpifs/var/ecset.F90
arpifs/var/ecset_thsafe.F90
arpifs/var/sugnss.F90
arpifs/op_obs/hjo.F90
arpifs/op_obs/map_varno_to_nvar.F90
arpifs/op_obs/hop.F90
arpifs/op_obs/obsop_gnss.F90
arpifs/op_obs/gnss_oberror.F90
arpifs/op_obs/gnss_slant_delay.F90
arpifs/op_obs/gnss_slant_delaytl.F90
arpifs/op_obs/gnss_slant_delayad.F90
arpifs/obs_preproc/suobs.F90
arpifs/obs_preproc/suobarea.F90
arpifs/obs_preproc/gnss_plane.F90
arpifs/obs_preproc/mkglobstab_obs.F90
arpifs/obs_preproc/prsta.F90
arpifs/obs_preproc/gefger.F90
arpifs/obs_preproc/black.F90
arpifs/obs_preproc/blackhat.F90
arpifs/obs_preproc/defrun.F90
arpifs/obs_preproc/fgchk.F90
arpifs/obs_preproc/first.F90
arpifs/obs_preproc/readoba.F90
arpifs/obs_preproc/sugoms.F90
arpifs/obs_preproc/pre_prsta.F90

B Flow chart of signal ray tracing

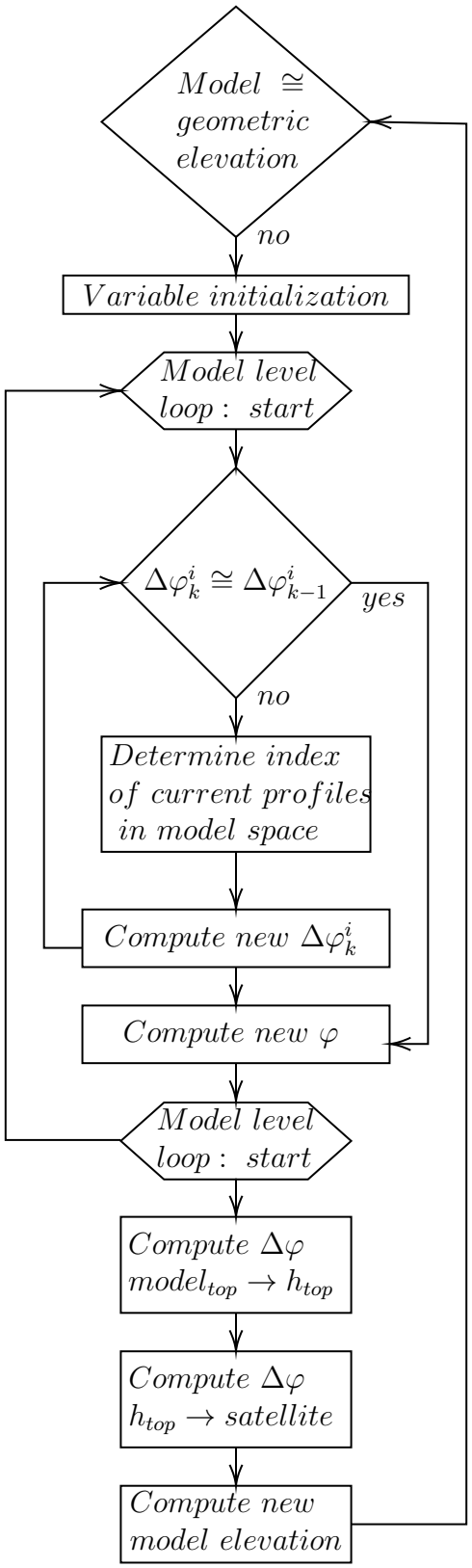

Figure 9: Ray tracing flow chart in the routine *gnss_slant_delay.F90*.